MIT Libraries | DSpace@MIT

MIT Open Access Articles

Design of a Thermally-Actuated Gas Lift Safety Valve

Massachusetts Institute of Technology

DESIGN OF A THERMALLY-ACTUATED GAS LIFT SAFETY VALVE

Eric Gilbertson
Department of Mechanical Engineering
Massachusetts Institute of Technology
Cambridge, Massachusetts 02139
Email: egilbert@mit.edu

Franz Hover
Department of Mechanical Engineering
Massachusetts Institute of Technology
Cambridge, Massachusetts 02139
Email: hover@mit.edu

Jose Arellano
Department of Reservoir and
Production Engineering
Chevron
Houston, Texas
Email: jaxx@chevron.com

Bryan Freeman
Completion Hardware Specialist
Chevron
Houston, Texas
Email: BryanFreeman@chevron.com

ABSTRACT

Gas-lifted oil wells are susceptible to failure through malfunction of gas lift valve assemblies (GLV). One failure mode occurs when the GLV check valve fails and product passes into the well annulus, potentially reaching the wellhead. This is a growing concern as offshore wells are drilled thousands of meters below the ocean floor in extreme temperature and pressure conditions, and repair and monitoring become difficult. Currently no safeguard exists in the GLV to prevent product passage in the event of check valve failure. In this paper a design and operational procedures are proposed for a thermally-actuated positive-locking safety valve to seal the GLV in the event of check valve failure. A thermal model of the well and GLV system is developed and compared to well data to verify feasibility of a thermally-actuated safety valve. A 3X scale prototype safety valve is built and tested under simulated failure scenarios and well start-up scenarios. Realistic well temperatures in the range of 20C to 70C are used. Results demonstrate valve closure in response to simulated check valve failure and valve opening during simulated well start-up.

Introduction

Gas lift is an artificial lifting method used to produce oil from wells that do not flow naturally. Gas is injected through the well annulus and into the well tubing at a down-well location (as shown in figure 1). The gas mixes with the oil in the tubing, aerating the oil and causing it to rise to the surface [2].

Gas lift valves are one-way valves that allow gas to pass from the annulus to the tubing but prevent oil from passing through to the annulus [2]. Most valves contain a pressurized bellows and an internal check valve (see figure 2). The bellows opens when the injection gas is pressurized above a threshold value, and the internal check valve prevents oil from passing through the gas lift valve [12] .

A gas lift valve fails if it allows oil passage from the tubing to the annulus [3]. Two main criteria must be met for failure to occur: (1) the reverse-flow check valve has a leak and the tubing pressure exceeds the gas pressure , (2) a combination of high tubing pressure and low gas pressure allows the bellows valve to open. See figure 2. Failure can also occur if both bellows and check valves leak, and tubing pressure exceeds annulus pressure.

The pressure relation that satisfies both of these criteria is described by the equation

$$P_{open} < P_{ann} < P_{tube} \tag{1}$$

where P_{open} is the annulus pressure required to open the bellows valve, P_{ann} is the actual pressure in the annulus, and P_{tube} is the pressure in the tubing.
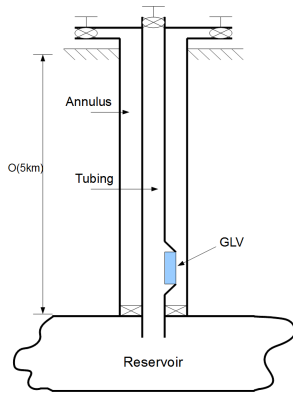
Figure 1. Schematic of oil well with gas lift valve (GLV). Top of figure represents sea floor.
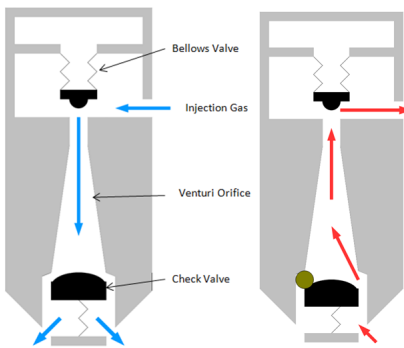

Figure 2. Gas lift valve model. Normal operation (left) and failure (right)

Proper function of gas lift valves is very important for the safety of the well and surface operations. If hydrocarbons flow through the wrong path (i.e. backflow from the tubing into the annulus, through a gas lift valve leak), they can reach the wellhead and create an undesired accumulation of high-pressure combustible material. Leaking gas lift valves are thought to have played a significant role in the 1988 accident on the Piper Alpha North Sea production platform, which led to an explosion and fire killing 167 men [10]. Even now, two decades after the Piper Alpha accident, gas lift valves are still susceptible to leakage [3], with seal corrosion being a major contributing factor.

Thus there is an opportunity for significantly improving the safety of production systems. Our view is that an additional valve, using temperature signaling, could offer such protection. Like the check valve, it can operate entirely without human interaction. Such a temperature-controlled valve could also add protection to other flow control devices, such as blowout preventers.

In this paper a design is proposed for a thermally-actuated gas lift safety valve that will prevent oil passage through the gas

lift valve in a failure scenario [8]. A steady state thermal model for the well is developed to study feasibility of a thermally-actuated valve. Model results are compared to experimental data, and the model used to predict gas-oil temperature differences. A 3X scaled prototype of the thermally-actuated gas lift safety valve is created and tested under heating and cooling scenarios to demonstrate full valve closure and full valve opening.
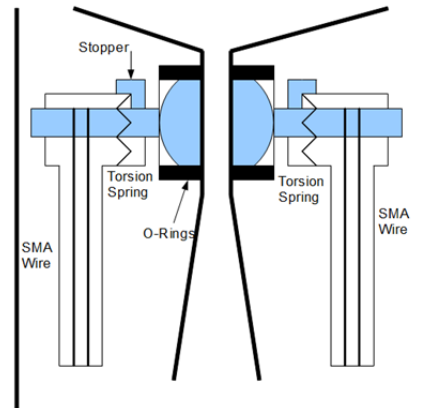
Thermally-Actuated Ball Valve Concept Details

Figure 3. Ball valve diagram. SMA wires contract to rotate valve closed. Wires expand and torsion spring rotates valve open.

Design Description

The thermally-actuated gas lift safety valve is a ball valve with cylindrical side extensions located in the top section of the venturi orifice of the gas lift valve, just below the bellows valve (see figures 3 and 4). The side extensions have small stoppers sticking out, which constrain the valve motion to 90 degrees of rotation between vertical (fully open) and horizontal (fully closed). The ball valve is supported by sliding bearings on the outside of the stoppers. The ball valve sits in a spherical pocket and relies on O-rings to form a water seal. The ball valve is actuated by shape memory alloy wires which are tied to the ball valve side extension, wrapped one-half revolution around the side extension, and attached to the gas lift valve housing below the side extension (see figure 3).

Shape memory alloys are alloys that undergo a solid state phase change between a Martensitic low-temperature state and an Austenitic high-temperature state when heated or cooled. These alloys are said to have memory because they return to the same low-temperature shape whenever cooled to the Martensitic state and to the same high-temperature shape when heated to the Austenitic state.
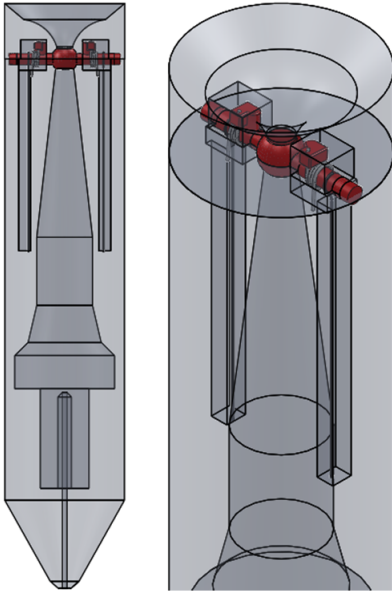
Figure 4.   Ball valve 3D picture

Shape memory alloys do not have a single transition temperature between Martensite and Austenite, but instead undergo a hysteresis, with different transition temperatures depending on whether the alloy is being cooled or heated. This hysteresis is shown schematically in figure 5, which plots strain vs temperature. In this figure, when the alloy is being heated A_s represents the start of the transition from Martensite to Austenite and A_f represents the final transition to Austenite. When being cooled, M_s represents the start of the transition from Austenite to Martensite and M_f represents the final transition to Martensite.
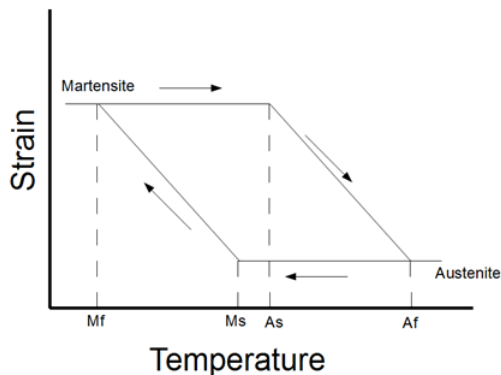

Figure 5.   Shape memory alloy hysteresis

Based on the alloy proportion, a shape memory alloy can have transition temperatures within the range of $-150°C$ to $+800°C$ [11]. In this thermally-actuated safety valve, the shape memory alloy is set to have a transition temperature A_s just above the gas temperature and A_f just below the oil temperature (shown in figure 8). The M_s and M_f transition temperatures are set to be between the oil temperature and the coldest temperature attainable in the valve-cooling scenario (described later in the operational procedures section, and in figure 8). If oil begins passing through the gas lift valve, the entire gas lift valve will heat up, in turn heating up the shape memory alloy wires to the oil reservoir temperature. The wires contract as they heat up past A_s and A_f, and will thus pull the ball valve into the closed position. Torsion springs are also wound around the ball valve side extensions. Thus, if the shape memory alloy cools and transitions to the Martensitic state, the wires will expand and the torsion springs will pull the ball valve back into the open position. Theoretically the valve could be actuated with shape memory alloy wire and torsion spring on only one side extension, but in this concept wire and torsion springs are located on both sides of the valve for redundancy.

Steady State Thermal Model

In order for a thermally-actuated positive locking device to be feasible using a shape memory alloy as the actuation element there must be sufficient temperature difference between the cold gas and hot oil to actuate the SMA. Commercially available shape memory alloys have a minimum hysteresis temperature spread of $6°C$ between A_s and A_f temperatures [9], and $15°C$ between A_f and M_f temperatures [9]. Thus there must be at least a $6°C$ temperature difference between gas and oil at injection depth during normal operation, and at least $15°C$ temperature difference between oil and gas temperature during cooling. Not all wells or locations in a given well will necessarily meet these criteria. Thus not every well is a candidate for the SMA-actuated safety valve technology, but it will be shown that this technology is still applicable to many wells.

In this section a model is derived for the steady state oil and gas temperature profiles in the well to determine the temperature difference between gas and oil at injection depth. This is a steady-state temperature model in space for the entire well.

Steady State Assumptions
Gas

- Steady state conditions
- Turbulent flow (100 <Nu< 1000 where Nu is the Nusselt number)
- Heating from ground and tubing by convection and conduction
- Surface gas temperature 300K
- Gas density is approximately constant down the annulus

3

Mixture

- Steady state conditions
- Turbulent flow ($100 < Nu < 1000$)
- Heat loss to annulus through convection and conduction
- Heat capacity and conductivity are weighted averages of gas and oil properties:

$$c_{mix} = \frac{\dot{m}_{gas}}{\dot{m}_{mix}} c_{gas} + \frac{\dot{m}_{oil}}{\dot{m}_{mix}} c_{oil} \qquad (2)$$

$$k_{mix} = \frac{\dot{m}_{gas}}{\dot{m}_{mix}} k_{gas} + \frac{\dot{m}_{oil}}{\dot{m}_{mix}} k_{oil} \qquad (3)$$

where c_{mix} is the specific heat of the gas-oil mixture, $\dot{m}_{gas}$ is the gas mass flow rate, $\dot{m}_{mix}$ is the mixture mass flow rate, c_{gas} is the gas specific heat, $\dot{m}_{oil}$ is the oil mass flow rate, c_{oil} is the oil specific heat, k_{mix} is the mixture thermal conductivity, k_{gas} is the gas thermal conductivity, and k_{oil} is the oil thermal conductivity.

- Mixture temperature at the injection point is a weighted average of gas and oil temperatures

$$T_{mix} = \frac{C_{gas}\dot{m}_{gas}}{C_{mix}\dot{m}_{mix}} T_{gas} + \frac{C_{oil}\dot{m}_{oil}}{C_{mix}\dot{m}_{mix}} T_{oil} \qquad (4)$$

where T_{mix} is the mixture temperature, T_{gas} is the gas temperature, and T_{oil} is the oil temperature.

Ground

- Linear temperature profile, slope 25K per Kilometer [7]
- Surface ground temperature = surface gas temperature

Piping

- Cement insulation around annulus, 10cm thick
- Steel tubing and annulus pipes 1cm thick

Modeling Approach

In figure 6 a control volume is drawn around a section of the well annulus between the depths of x and $x + dx$. For simplicity the control volume of the half of the annular segment is represented in 2 dimensions as a rectangle, where R_{case} is the casing inner radius, R_{tube} is the tubing inner radius, $R_{case} - R_{tube}$ is the width of the differential element, and dx is the height of the differential element. Heat is transferred into the control volume by convection and conduction through the casing wall, convection

and conduction through the tubing wall, and mass flow into the top of the control volume. Heat is transferred out of the control volume through mass flow out the bottom of the volume.
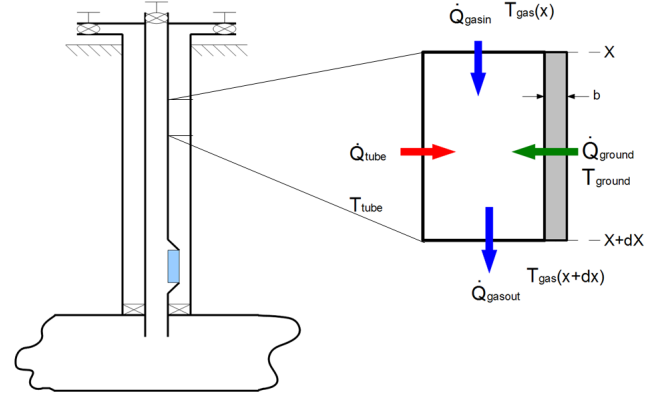

Figure 6.   Heat transfer model for annulus control volume

Heat transfer from the casing to the gas is given by

$$\dot{Q}_{ground} = \frac{\left(T_{ground}(x) - T_{gas}(x)\right)}{R_{totg}} \qquad (5)$$

where $\dot{Q}_{ground}$ is the heat transfer from the casing to the control volume, $T_{ground}(x)$ is the ground temperature at depth x, and $T_{gas}(x)$ is the gas temperature at depth x. R_{totg} is the total thermal resistance across the casing interface, which is the sum of the conduction and convection resistances,

$$R_{totg} = \frac{b}{k_{cem} 2\pi R_{case} dx} + \frac{1}{h_{ground} 2\pi R_{case} dx} \qquad (6)$$

where b is the casing wall thickness, k_{cem} is the cement thermal conductivity, h_{ground} is the convective heat transfer coefficient of the casing wall, and R_{case} is the casing radius.

In these equations the ground temperature in Kelvins is assumed to be of the form

$$T_{ground}(x) = 273 + \frac{1}{40}x \qquad (7)$$

where x is measured in meters below the surface [7]. The convective heat transfer coefficient is given by

$$h_{ground} = \text{Nu} \frac{k_{gas}}{2R_{case}} \qquad (8)$$

Heat transfer from the tubing to the gas is given by

$$\dot{Q}_{tube} = \frac{(T_{tube}(x) - T_{gas}(x))}{R_{tott}} \qquad (9)$$

where $\dot{Q}_{tube}$ is the heat transfer from the tubing to the annulus, and $T_{tube}(x)$ is the tubing temperature at depth x. R_{tott} is the total thermal resistance across the tubing interface, which is the sum of the conduction and convection resistances,

$$R_{tott} = \frac{a}{k_{tube}2\pi R_{tube}dx} + \frac{1}{h_{tube}2\pi R_{tube}dx} \qquad (10)$$

where a is the tubing wall thickness, k_{tube} is the tubing wall thermal conductivity, R_{tube} is the tubing radius, and h_{tube} is the convective heat transfer coefficient of the tubing wall given by

$$h_{tube} = \text{Nu} \frac{k_{mix}}{2R_{tube}} \qquad (11)$$

Heat transfer through the control volume due to mass flow is given by

$$\dot{Q}_{outgas} - \dot{Q}_{ingas} = \dot{m}_{gas}c_{gas}\left(T_{gas}(x+dx) - T_{gas}(x)\right) \qquad (12)$$

where $\dot{Q}_{outgas}$ is the heat transfer out the bottom of the control volume due to mass flow, $\dot{Q}_{ingas}$ is the heat transfer into the control volume due to mass transfer, $\dot{m}_{gas}$ is the gas mass flow rate, and c_{gas} is the gas specific heat.

The gas mass flow rate is calculated by

$$\dot{m}_{gas} = \frac{\rho_{gas}}{\rho_{oil}} R_s \dot{m}_{oil} \qquad (13)$$

where ρ_{gas} is the gas density, ρ_{oil} is the oil density, and R_s is the gas-oil volumetric ratio at injection depth. The gas density can be calculated using the ideal gas law, assuming constant gas density from the surface,

$$\rho_{gas} = \frac{P_{gas}M_{gas}}{RT_{gassurf}} \qquad (14)$$

where P_{gas} is the surface gas pressure, M_{gas} is the gas molar mass, R is the ideal gas constant, and $T_{gassurf}$ is the surface gas temperature.

An energy balance for the control volume yields the equation

$$\dot{Q}_{outgas} - \dot{Q}_{ingas} = \dot{Q}_{tube} + \dot{Q}_{ground} \qquad (15)$$

Combining equations 12 and 15, dividing both sides by dx, and taking the limit as dx goes to zero yields the differential equation

$$\dot{m}_{gas}c_{gas}\frac{dT_{gas}(x)}{dx} = \frac{T_{tube}(x) - T_{gas}(x)}{B_1} + \frac{T_{ground}(x) - T_{gas}(x)}{B_2} \qquad (16)$$

where

$$B_1 = \frac{a}{k_{tube}2\pi R_{tube}} + \frac{1}{h_{tube}2\pi R_{tube}} \qquad (17)$$

and

$$B_2 = \frac{b}{k_{cem}2\pi R_{case}} + \frac{1}{h_{ground}2\pi R_{case}} \qquad (18)$$

Using similar derivation methods, a differential equation can be derived for a control volume in the tubing.

The differential equation describing the tubing temperature is

$$\dot{m}_{mix}c_{mix}\frac{dT_{tube}(x)}{dx} = \frac{(T_{tube}(x) - T_{gas}(x))}{\frac{a}{k_{tube}2\pi R_{tube}} + \frac{1}{h_{tube}2\pi R_{tube}}} \qquad (19)$$

The Runge Kutta numerical integration technique is used to solve the pair of differential equations 19 and 16 to generate temperature profiles in the annulus and tubing. For each solution a bottom well mixture temperature is guessed and solution profiles generated. When the surface temperature of the annulus profile equals surface air temperature, the algorithm stops.

Parameter	Value	Units	Source
w	2500	m	Well Data
$\dot{m}_{mix}$	24	$\frac{kg}{s}$	Well Data
$\dot{m}_{gas}$	16.5	$\frac{kg}{s}$	Well Data
c_{gas}	2500	$\frac{J}{kgK}$	[4]
a	0.01	m	[2]
k_{tube}	50	$\frac{W}{mK}$	[1]
R_{tube}	0.0508	m	Well Data
b	0.362	m	[2]
k_{cem}	1.73	$\frac{W}{mK}$	[1]
R_{case}	0.1016	m	Well Data
c_{oil}	1841	$\frac{J}{kgK}$	[4]
k_{oil}	0.15	$\frac{W}{mK}$	[4]
k_{gas}	0.04	$\frac{W}{mK}$	[4]
T_{res}	356	K	Well Data
$T_{gassurf}$	300	K	Well Data
R_s	45	Unitless	Well Data

Table 1.   Parameter values

Comparison with Experimental Data

To check the validity of the model, temperature profiles were compared to data from an actual well. A well temperature survey was provided by Chevron where data is for the temperature inside the tubing. Of the 17 parameters required for the model, 8 were provided by Chevron and 8 were standard values looked up in other sources (such as oil specific heat, oil thermal conductivity, etc.) (see table). The only unknown parameter was the Nusselt number of the well. The flow was assumed to be turbulent with a Nusselt number between 100 and 1000, and different Nusselt numbers were tried until the model matched the data.

Figure 7 shows the steady state well temperature profiles for a Nusselt number of 675, which yields good agreement between model and data. The temperature model was then expanded to describe a subsea well, with an exponential model assumed for ocean temperature vs depth [6] and an ocean depth of 1000m assumed. The well injection depth is 3000m below the sea bottom. Resulting plots with and without the tubing subsurface safety valve closed and a Nusselt number of 675 are plotted in figures 8 and 9 respectively.
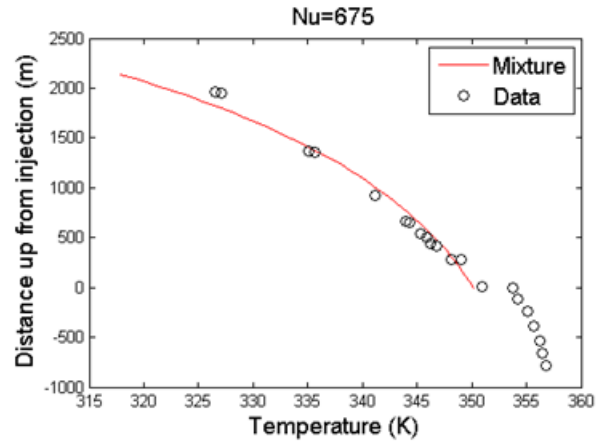

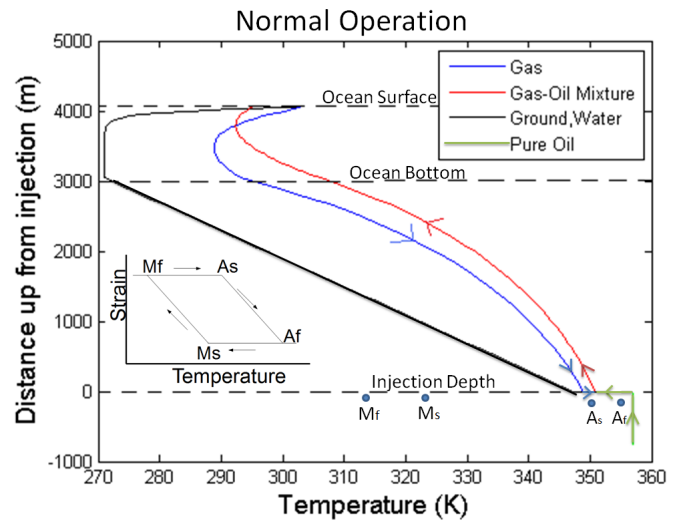Figure 7.   Steady state tubing and annulus temperature profiles

Figure 8.   Steady state tubing and annulus temperature profiles with tubing safety valve open. Direction of flow is shown for gas, oil, and mixture. Ideal shape memory alloy transition temperatures shown relative to gas and oil temperatures at injection depth. This figure shows the gas lift valve assembly will be at 349K during normal operation (gas temperature at injection depth, less than A_s), and 357K after a failure scenario (oil temperature at injection depth, greater than A_f. Thus the valve will completely close.

These plots show that there is an eight-degree temperature difference between gas and reservoir oil temperature at injection depth with the tubing safety valve open, and a 55 degree temperature difference with the tubing safety valve closed. Thus enough temperature difference exists to actuate shape memory alloys in the thermally-actuated gas lift safety valve.
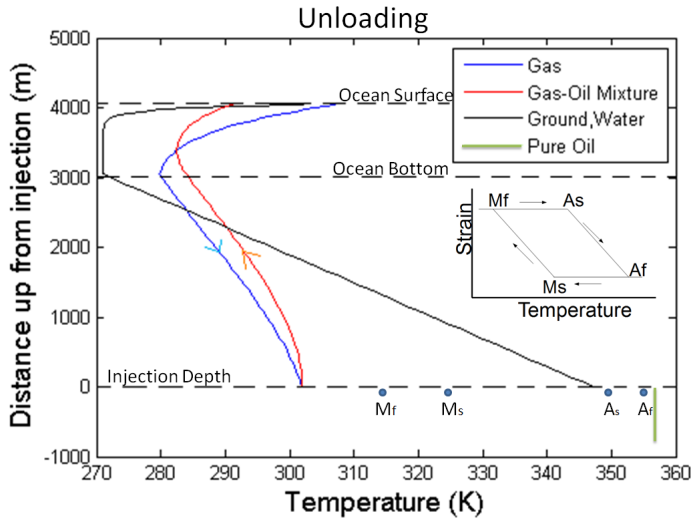
Figure 9. Steady state tubing and annulus temperature profiles with tubing safety valve closed and gas passing through the bottom GLV at the end of an unloading procedure.Direction of flow is shown for gas, oil, and mixture. Ideal shape memory alloy transition temperatures shown relative to gas and oil temperatures at injection depth. This figure shows gas lift valve assembly will be at 302K, which is less than the transition temperature M_f. Thus the valve will completely open.

Operational Procedure

Unloading Only the gas lift valve at operating depth contains the thermally-actuated ball valve (referred to subsequently as thermal valve). The operating valve is the second lowest in the tubing, with an additional standard unloading valve located below the operating valve. The bellows of the thermal valve is pressurized to a lower value than all of the other GLV bellows in the system. During the unloading process the additional lower unloading valve is used to cool the thermal valve, as detailed in figures 10. In this operational procedure the tubing subsurface safety valve is closed for the duration of the unloading process to allow better convective cooling of the thermal valve.

Initially the thermal valve is at the hot steady-state oil temperature and the thermal valve is closed. As a result, the thermal valve initially acts like a dummy valve and the unloading occurs exactly as normal until only the bottom valve is passing gas. At this point, gas is flowing past the thermal valve on the annulus side and on the tubing side (because the tubing safety valve is closed and no oil is entering the system) and the thermal valve cools by convection. When the thermal valve cools sufficiently below the Martensitic transition temperatures M_s and M_f, it begins to open and pass gas. Gas now flows through a larger total area (the bottom two valves), and the annulus pressure thus drops. This causes the bottom gas lift valve to close. The thermal valve bellows is pressurized to a lower pressure than the bottom gas lift valve and thus stays open passing gas. Now only the ther-
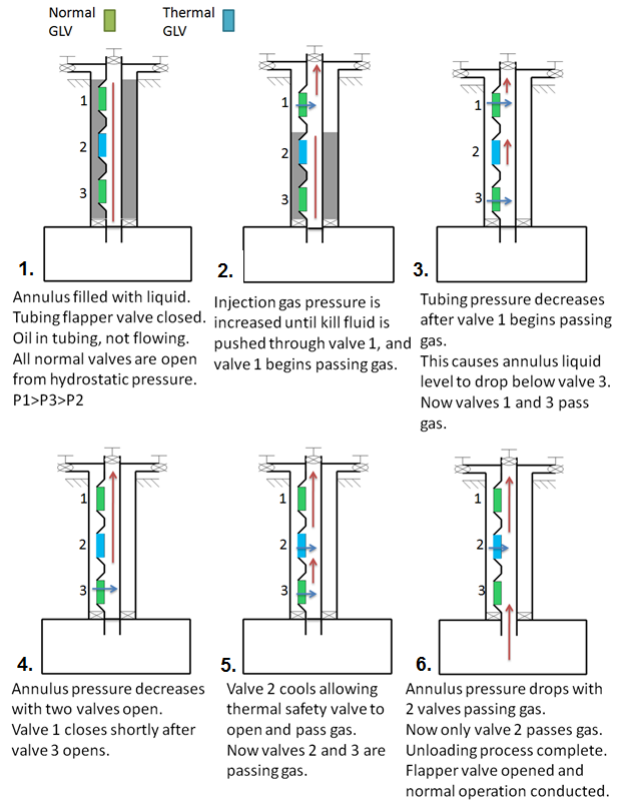

Figure 10. Schematic 3-valve unloading process with thermal valve

mal valve is passing gas as desired. The tubing subsurface safety valve is now opened and normal production begins.

The thermal valve is located approximately 15m above the bottom unloading valve so that it is far enough above to be retrieved by wireline techniques with current wireline accuracies, but not far enough to significantly affect well production rates. In normal continuous-flow operation gas flows through the thermal valve while all other gas lift valves remain closed.

Single-point intermittent gas lift is also possible with the thermal valve. If the cycling time between gas injections is sufficiently short to leave the thermal valve colder than A_s, then the intermittent lifting process will be unaffected by the thermal valve. Simple modeling shows this time to be approximately 40 minutes [8]. If the cycling time is not sufficiently short, then the shut-in process, described in the next section, would need to be followed to reopen the valve before every injection.

Shut-in During a shut-in, when injection of gas into the annulus is stopped, the thermal valve will heat up or cool down to a steady state temperature dependent on the oil temperature and ground temperature. If the valve heats up to a temperature greater than the transition temperature of the thermal valve, the ball valve will close. When the shut-in is complete, gas is injected first

7

through the bottom unloading valve. The air circulates past the thermal valve, cooling it down. When the thermal valve cools below its transition temperature it opens and begins passing gas. Because gas is now passing through a larger combined opening, the gas pressure drops and the lower gas lift valve closes. Thus the thermal valve is the only valve passing gas, and normal well production resumes.

Prototype

A scaled prototype positive lock is created and tested under simulated oil well temperatures. The purpose of the prototype is to demonstrate that the ball valve will completely close when the SMA wires are heated by conduction (in this case using temperature-controlled water) above the Austenitic transition temperature A_f and completely open when SMA wires are cooled below the Martensitic transition temperature M_f. Future tests should focus on heating and cooling the SMA wires by conduction through a metal housing . For ease of machining the prototype is constructed out of plastic at a 3X scale from the dimensions of an XL-175 gas lift valve. The top part of the prototype is constructed out of clear acrylic to allow valve actuation to be seen, while the bottom section is constructed out of Delrin because of its ease in machining. The prototype housing consists of a cylinder representing the section of the gas lift valve between the check valve and the bellows valve (see figure 11)

A straight cylindrical hole is located vertically through the housing for liquid to pass through. A second side hole is located next to the central hole extending from the bottom of the housing to the ball valve side extension. This second hole allows hot water to flow over and heat up the shape memory alloy wire. A connecting hole allows hot liquid to flow from the shape memory alloy hole back into the main gas lift valve orifice. In the actual valve the shape memory alloy wire will heat up over time through conduction of the metal housing, but for the plastic prototype this heating is simulated by allowing the wire to contact the hot liquid to heat up.

The housing is cut horizontally into three sections. The ball valve is located between the top two sections with the connecting hole located between the middle and bottom sections. The valve is actuated only on one side by Nitinol wires. The Nitinol wire used is Flexinol brand, A_s stated transition temperature 70C, produced by Dynalloy [5]. Though the Flexinol used does not have the tight hysteresis spreads that will be needed in the final implementation of the valve, Flexinol is easily commercially available and sufficient to demonstrate proof of concept prototype testing at realistic shallow oil well temperatures (in this case up to 70C).

The Nitinol is attached to the ball valve side extension as described earlier. The wire is then wrapped one half revolution around the ball valve side extension and passes through the side hole to the bottom of the housing. The bottom end of the wire is fixed to the prototype housing via a bolt passing horizontally into the housing (see figure 11). The bolt presses the wire against the housing side, securing it in place. Both attachment methods are recommended by Dynalloy for attaching shape memory alloy wires.

Tight seals are created at the entrance and exit of the ball valve by using rubber O-rings. The ball valve sits in a cylindrical cavity with O-rings on the top and bottom that deform to press tightly against the ball valve (see figure 11).
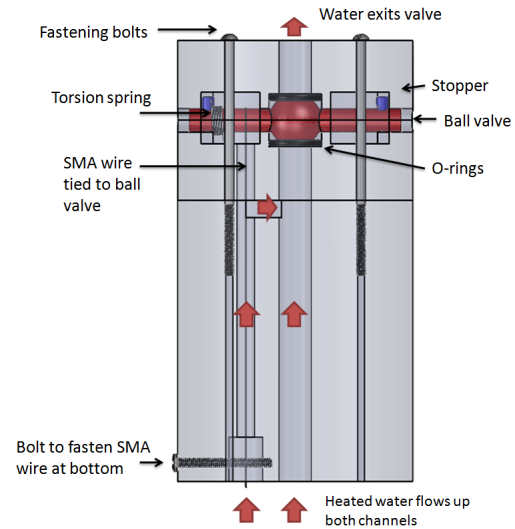

Figure 11.   Prototype valve fluid flow diagram

Experimental Setup

The experimental setup is designed to test the actuation temperature and hysteresis behavior of the prototype valve and to act as a proof of concept of the thermally-actuated ball vale. A schematic diagram of the setup is shown in figure 12.

Water is pumped from a storage tank, through a water heater, through the prototype valve, and back into the water storage tank. A pressure relief valve is located on the input side of the prototype valve to allow water to pass around when the positive lock closes. A thermocouple senses the water temperature at the valve outlet. A tilt sensor is mounted to the ball valve end extension to record the ball valve position.

A pressure transducer is mounted near the pump outlet to allow closed-loop control of the pump speed. Pipes are made of aluminum because of its ability to withstand temperatures in excess of 70C as are necessary to heat up the SMA wire.

The Labview software/hardware program is used to acquire data from the sensors and supply necessary power for the sensors. The water heater is plugged into a standard 120VAC wall outlet.
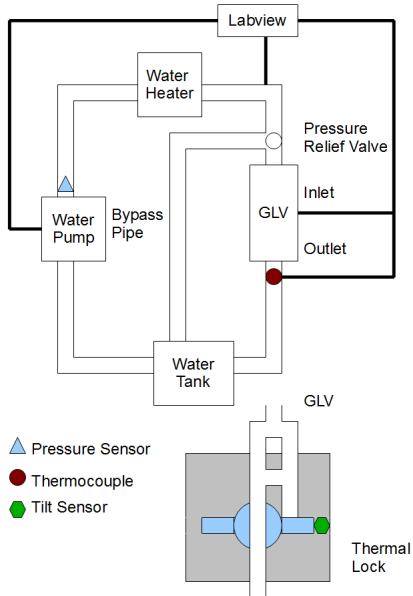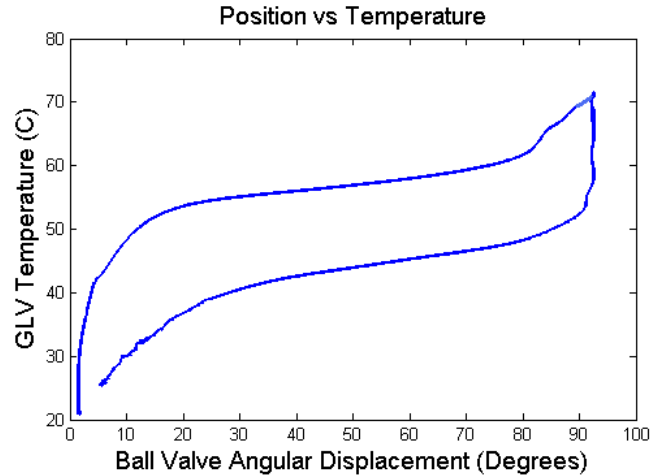
Figure 12.   Schematic of experimental setup

Figure 13.   Ball valve hysteresis

The centrifugal pump is supplied with a closed-loop PID controller that relies on a pressure measurement at the pump outlet to control the flow. The set pressure of the controller is manually input as desired.

Experimental Results

Figure 13 shows an angular displacement hysteresis plot of the ball valve as a function of temperature for a typical experimental trial (ie, heating above A_f, then cooling below M_f) at realistic well temperatures. Data is filtered by a standard second-order butterworth low pass filter with normalized cutoff frequency 0.003 to reduce noise.

The hysteresis plot shows that the ball valve begins closing when heated to an A_s temperature of approximately 50C and finishes closing at an A_f temperature of approximately 60C. The ball valve begins opening when cooled to an M_s temperature of approximately 50C and finishes opening at an M_f temperature of approximately 30C. The ball valve started at an angle of 0 degrees, completely closed to an angle of 90 degrees, and then completely opened.

Discussion of Results

The experimental results show that it is possible to thermally actuate a ball valve through conductive heating of shape memory alloy wires to turn completely closed with 90 degrees of angular displacement, and to thermally actuate the valve to completely reopen to its original position. The results thus show that the shape-memory-alloy thermally-actuated ball safety valve is a

feasible design applicable at realistic oil well temperatures.

For the particular parameters and shape memory alloy used in this experiment, a well would need a gas-oil temperature difference at injection depth of at least 10C for the safety valve to close in a backflow scenario. The well data shown in Figure 7, which is typical based on several well surveys examined, shows a temperature difference of about 5C between mixture and oil. Several more degrees could be expected between gas temperature and mixture temperature (though this data was not provided), giving a typical gas-oil temperature difference of 5C-10C. Thus the well in Figure 7 could possibly be a candidate for a thermal safety valve with the given alloy and parameter values. Other commercially available shape memory alloys with A_s-A_f spreads as low as 6C could be used to ensure that the well in Figure 7 would be a suitable candidate for the thermally-actuated safety valve.

Ongoing work is focusing on further reducing the A_s-A_f temperature spread of the safety valve by modifying friction and spring torque behavior of the design. This will allow the safety valve to be applicable to wells with even smaller gas-oil temperature differences. Additional future work should focus on more realistic materials (such as stainless steel), robustness, and reliability.

Acknowledgments

Nomenclature

Symbol	Definition	Units
w	Well Depth	m
$\dot{m}_{mix}$	Mixture mass flow rate	$\frac{kg}{s}$
$\dot{m}_{gas}$	Gas mass flow rate	$\frac{kg}{s}$
c_{gas}	Gas specific heat	$\frac{J}{kgK}$
a	Tubing wall thickness	m
k_{tube}	Tubing wall conduction coefficient	$\frac{W}{mK}$
R_{tube}	Tubing radius	m
b	Casing wall thickness	m
k_{cem}	Casing conduction coefficient	$\frac{W}{mK}$
R_{case}	Casing radius	m
c_{oil}	Oil specific heat	$\frac{J}{kgK}$
k_{oil}	Oil conduction coefficient	$\frac{W}{mK}$
k_{gas}	gas conduction coefficient	$\frac{W}{mK}$
T_{res}	Reservoir temperature	K
$T_{gassurf}$	Surface gas temperature	K
R_s	Gas-oil volumetric ratio at injection depth	Unitless
$\dot{Q}_{ground}$	Ground heat flow rate	W
$\dot{Q}_{tube}$	Tubing-to-annulus heat flow rate	W
$\dot{Q}_{ingas}$	Heat flow rate into gas control volume	W
$\dot{Q}_{outgas}$	Heat flow rate out of gas control volume	W
Nu	Nusselt number	unitless
x	Distance from injection depth	m
T_{tube}	Tubing temperature	K
T_{gas}	Gas temperature	K
R_{totg}	Thermal resistance across casing	$\frac{K}{W}$
R_{tott}	Thermal resistance across tubing	$\frac{K}{W}$
c_{mix}	Mixture specific heat	$\frac{J}{kgK}$
k_{mix}	Mixture conduction coefficient	$\frac{W}{mK}$
T_{mix}	Mixture temperature	K
h_{ground}	Ground convection coefficient	$\frac{W}{m^2K}$
ρ_{gas}	Gas density	$\frac{kg}{m^3}$
ρ_{oil}	Oil density	$\frac{kg}{m^3}$
P_{gas}	Gas pressure	Pa
R	Ideal gas constant	$\frac{J}{molK}$

REFERENCES

[1] M.F. Ashby. *Materials Selection in Mechanical Design*. Pergamon Press Ltd, 1996.

[2] Kermit Brown. *The Technology of Artificial Lift Methods, vol 2A*. The Petroleum Publishing Company, 1980.

[3] Jorn Andre Carlsen, Oyvind Stokka, and Erling Kleppa. Taking the Gas Lift Valves to a New Level of Reliability. In *Offshore Technology Conference, Houston, TX, USA*, May 2010.

[4] DK Das, S Nerella, and D Kulkarni. Thermal properties of petroleum and gas-to-liquid products. *Petroleum Science and Technology*, 25(4):415–425, April 2007.

[5] Dynalloy. Dynalloy Inc. Makers of Dynamic Alloys. http://www.dynalloy.com, 2010.

[6] A. I. Felzenbaum. Exponential Model of the Seasonal Thermocline. *Physical Oceanography*, 3(1), 1992.

[7] I.B. Fridleifsson, R. Bertani, E. Huenges, J.W. Lund, A. Ragnarsson, and L. Ryback. The possible role and contribution of geothermal energy to the mitigation of climate change, Luebck, Germany. In *IPCC SCoping Meeting on Renewable Energy Sources*, January 2008.

[8] Eric Gilbertson. Gas lift valve failure mode analysis and the design of a thermally-actuated positive-locking safety valve. Master's thesis, Massachusetts Institute of Technology, 2010.

[9] Dimitris Lagoudas. *Shape Memory Alloys: Modeling and Engineering Applications*. Spring Science+Business Media, LLC, 2008.

[10] M. Elisabeth Pate-Cornell. Learning from the Piper Alpha Accident: A Postmortem Analysis of Technical and Organizational Factors. *Risk Analysis*, 13(2):215–232, 1993.

[11] F. Sczerzenie. Consideration of the ASTM Standards for NiTi Alloys. In *Proceedings of the International Conference on Shape Memory and Superelastic Technologies, Baden-Baden Germany* , October 2004.

[12] Gabor Takacs. *Gas Lift Manual*. Pennwell Corporation, 2005.